



LAWRENCE
LIVERMORE
NATIONAL
LABORATORY

Soft x-ray images of the Laser Entrance Hole of NIC Hohlraums (paper, HTPD2012)

M. B. Schneider, N. B. Meezan

May 3, 2012

High Temperature Plasma Diagnostics
Monterey, CA, United States
May 6, 2012 through May 10, 2012

Disclaimer

This document was prepared as an account of work sponsored by an agency of the United States government. Neither the United States government nor Lawrence Livermore National Security, LLC, nor any of their employees makes any warranty, expressed or implied, or assumes any legal liability or responsibility for the accuracy, completeness, or usefulness of any information, apparatus, product, or process disclosed, or represents that its use would not infringe privately owned rights. Reference herein to any specific commercial product, process, or service by trade name, trademark, manufacturer, or otherwise does not necessarily constitute or imply its endorsement, recommendation, or favoring by the United States government or Lawrence Livermore National Security, LLC. The views and opinions of authors expressed herein do not necessarily state or reflect those of the United States government or Lawrence Livermore National Security, LLC, and shall not be used for advertising or product endorsement purposes.

Soft x-ray images of the Laser Entrance Hole of NIC Hohlräume^{a)}

M. B. Schneider^{1b)}, N.B. Meezan¹, S.S. Alvarez¹, J. Alameda¹, S. Baker¹, P. M. Bell¹, D.K. Bradley¹, D.A. Callahan¹, J. R. Celeste¹, E. L. Dewald¹, S.N. Dixit¹, T. Doeppner¹, D. C. Eder¹, M.J. Edwards¹, M. Fernandez-Perea¹, E. Gullikson⁵, M.J. Haugh², S. Hau-Riege¹, W. Hsing¹, N. Izumi¹, O. S. Jones¹, D. H. Kalantar¹, J.D. Kilkenny⁴, J.L. Kline³, G.A. Kyrala³, O.L. Landen¹, R.A. London¹, B.J. MacGowan¹, A.J. MacKinnon¹, T. J. Mccarville, J.L. Milovich¹, P. Mirkarimi¹, J.D. Moody¹, A.S. Moore⁶, M. D. Myers¹, E.A. Palma¹, N. Palmer¹, M.J. Pivovarov¹, J. E. Ralph¹, J. Robinson¹, R. Soufli¹, L. J. Suter¹, A.T. Teruya¹, C.A. Thomas¹, R.P. Town¹, S.P. Vernon¹, K. Widmann¹, B.K. Young¹

¹Lawrence Livermore National Laboratory, P.O. Box 808, Livermore, CA 94551-0808 USA

²National Security Technologies, PO Box 2710, Livermore, CA 94550 USA

³Los Alamos National Laboratory, Los Alamos, NM 87545 USA

(Presented XXXXXXXXXXXXXXXXXXXX; received XXXXXXXXXXXX; accepted XXXXX; published online XXXXX)

Hohlräume at the National Ignition Facility convert laser energy into a thermal x-radiation drive, which implodes the capsule, thus compressing the fuel. The x-radiation drive is measured with a low resolution, time-resolved x-ray spectrometer that views the hohlraum's laser entrance hole (LEH) at 37° to the hohlraum axis. This measurement has no spatial resolution. To convert this to the drive inside the hohlraum, the area and fraction of the measured x-radiation which comes from the region inside the hohlraum must be known. The size of the LEH is measured with the time integrated Static X-ray Imager (SXI) which view the LEH at 18° to the hohlraum axis. A soft x-ray image has been added to the SXI to measure the fraction of x-radiation inside the LEH's Clear Aperture in order to correct the measured radiation. A multilayer mirror plus filter selects an x-ray band centered at 870 eV, near the x-ray energy peak of a 300 eV blackbody. Results from this channel and corrections to the x-radiation drive are discussed.

I. Introduction

The goal of experiments at the National Ignition Facility (NIF)¹ is to achieve ignition through the indirect drive technique.² Figure 1 shows a schematic of the target and laser beams used in the current experiments.³ The target is a gas-filled, cryogenic hohlraum with a plastic capsule at its center. The capsule is filled with helium gas doped with deuterium and tritium³⁻⁴. Ninety-six laser beams, sixty-four in outer cones (50°, 44.5°) and thirty-two in inner cones (30°, 23.5°) enter the laser entrance holes (LEH) at each end of the hohlraum in 20 ns shaped pulses with total energies ranging from 1.2 to 1.65 MJ with wavelength 351 nm. The laser energy is converted into x-ray energy via the inverse bremsstrahlung interaction with the gas fill or the high-Z hohlraum walls. The x-ray drive heats and ablates the outer shell of the capsule, thereby compressing the inner core.²⁻⁴ It is important to understand the coupling of the x-radiation drive to the capsule. The first step is to obtain an accurate measurement of the x-radiation drive.

The radiation drive is measured with DANTE⁵, a low resolution, time-resolved x-ray spectrometer. DANTE views the Laser Entrance Hole (LEH) at 37° to the hohlraum axis.

Measurements of the size of the LEH's Clear Aperture and the fraction of flux coming from INSIDE the Clear Aperture are used to convert DANTE measurement to the x-radiation drive inside the hohlraum.

The Static X-ray Imager (SXI)⁶⁻⁷ captures time-integrated pictures of the inside of the hohlraum as viewed through the LEH. Its observation angle is 18° (upper SXI) or 19° (lower SXI) to the hohlraum axis (Figure 1). The images provide information on the backlit size of the LEH. However, to correctly interpret the x-radiation flux measurements, the fraction of the flux coming from inside the Clear Aperture must be known. We have built a new soft x-ray channel to measure this. The channel is composed of a multilayer mirror and thin filter. It produces an x-ray image centered at 870 eV, near the peak x-ray energy of a 300 eV blackbody.

We describe here the soft x-ray channel including the multilayer mirror. We describe how the image is used to correct the measured x-radiation flux. A further use of the image to directly indicate radiation temperature is also described.

II. The SXI diagnostic and soft channel

The upper SXI⁶ diagnostic views the LEH at an angle of

^{a)}Contributed paper published as part of the Proceedings of the 19th Topical Conference on High-Temperature Plasma Diagnostics, Monterey, CA, May, 2012.

^{b)}Author to whom correspondence should be addressed. Electronic mail: schneider5@llnl.gov

18° to the hohlraum axis. It is operated at 2X magnification with the detector situated at 4.88 m from the target. The detector is an x-ray sensitive, thinned, back-illuminated silicon CCD.⁸ The silicon substrate is 15 μm thick, with 24 μm square pixels in a 2k x 2k array. The detector is absolutely calibrated.⁸ The CCD is mounted at the end of a moveable stage (boom) that is a cylinder 82.5 mm in diameter.⁷

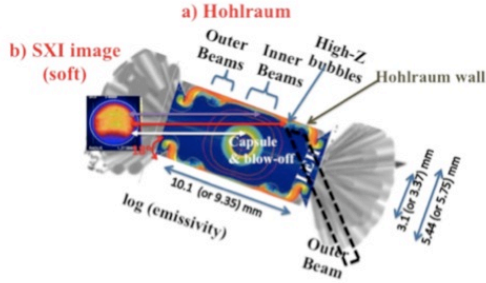


Figure 1: Schematic of the experimental set-up. The hohlraum axis is tilted 18° to SXI image. a) Sketch of hohlraum showing laser beams (on outside) and HYDRA³ simulation of emissivity at 900 eV on the inside. The places where the beams hit the wall at early time are identified. Not shown is the trajectory of the laser beams inside the hohlraum. One outer beam is shown in dashes to illustrate that a high-Z bubble is formed where the outer beams hit the wall. b) Typical SXI image: The purple arrow connects the feature in the SXI image to an inner beam. The red arrow connects the feature in the SXI image to the high-Z bubble created by outer beams. The white arrow connects faint feature at the bottom of the SXI image to capsule blow-off.

The soft x-ray channel design was a retrofit into the existing SXI boom tube. The final design is shown in Figure 2. It uses a 10° angle of incidence multilayer mirror plus a light tight filter consisting of 2 μm thick copper and 1 μm thick polyimide.

The multilayer mirror consists of alternating layers of tungsten and boron carbide on a 0.7 mm thick silicon substrate. The bottom layer is tungsten. Each tungsten layer is 21.55 Å thick and the total thickness of the bilayer is 43.1 Å. There are 30 bilayers and a 40 Å thick silicon carbide “capping layer” on the top to prevent oxygen diffusing into the layers and creating oxides. The performance of the multilayer was verified at the Advance Light Source (ALS) by measuring the reflectivity vs angle at ~1 keV x-ray energy.⁹

Figure 3a shows the reflectivity of the multilayer mirror and Figure 3b shows the throughput of the multilayer mirror plus the

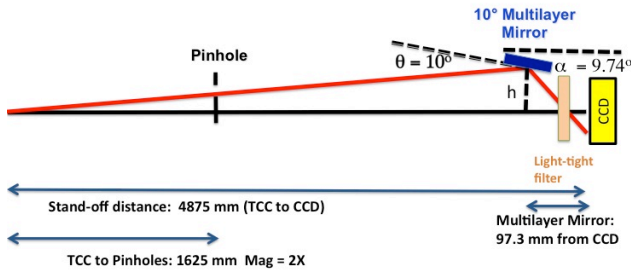


Figure 2: Optical path for the soft x-ray channel. The design was retrofitted into the SXI so the mirror had to be inserted into SXI boom from the CCD end and it had to be close enough to SXI axis to clear the tube of the boom. This led to a 10° angle-of-incidence design.

filter. The filter is needed to cut out low energy x-rays and the

higher orders. The pinhole diameter, 45 μm , is chosen so that the contributions of diffraction and geometry are about equal in this x-ray range. (CHECK)

Figure 4 shows typical SXI data: a hard x-ray image in the 3-5 keV range and a soft image at x-ray energy of 870 eV. In this shot, 1.XX MJ was fired into a hohlraum whose LEH was 3.1 mm.

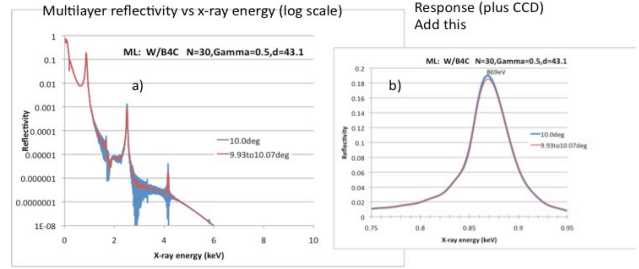


Figure 3: a) Multilayer reflectivity (log scale) b) Response of soft x-ray channel

III. Results

The image from the hard channel is used to determine the Clear Aperture.⁶ The image from the soft channel is used to ascertain the fraction of thermal x-radiation flux inside the Clear Aperture.

The Clear Aperture is obtained from a 0.3 mm wide horizontal lineout from the hard x-ray image and from a radial distribution function (RDF). To calculate the RDF, the image is made circular by stretching it vertically around the LEH center by $1/\cos(18^\circ)$. The average counts in circular rings about the center of the LEH are calculated. The horizontal lineout (black) and the RDF (red) are plotted Figure 5a. The Clear Aperture size is the average of the midpoints of the steep slope of the horizontal lineout and the RDF. Figure 4 plots the Clear Aperture over the original SXI images.

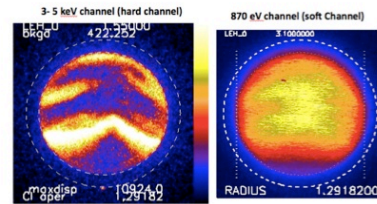


Figure 4: Typical SXI data. (a) Image at x-ray energy of 3-5 keV; (b) Image at x-ray energy of 870 eV. The original LEH diameter (3.1 mm) is the outer dashed light. The inner dashed line is the Clear Aperture as determined from (a).

In the same manner, a radial distribution function is also calculated for the 870 eV image. The RDF is normalized by dividing by the total counts in the image. The cumulative distribution function (CDF) is calculated as the running sum of counts within a given radius versus radius. The fraction of counts within the radius of the Clear Aperture is then determined. Figure 5b shows the RDF (black) and the CDF (red).

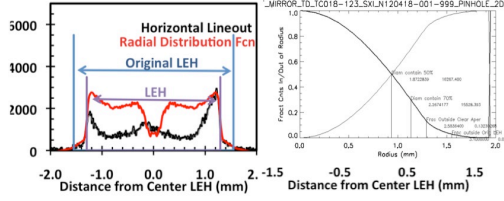


Figure 5: Lineouts. (a) Horizontal lineout (black) and RDF (red) from 3-5 keV channel (Figure 4a) used to obtain the Clear Aperture. (b) RDF (black) and CDF (red) from 870 eV channel (Figure 4b) used to obtain f , the fraction of energy inside the Clear Aperture. (Incorrect picture, will fix later)

IV. DANTE Correction

The x-radiation drive, or flux, F_{DANTE} is directly measured by the DANTE diagnostic.³⁻⁵ It is converted to a radiation temperature, T_{DANTE} , by

$$F_{\text{DANTE}} = \sigma T_{\text{DANTE}}^4 \pi R_{\text{LEH}}^2 \cos \theta \quad (1)$$

where θ is 37° , the angle of the DANTE view to the hohlraum axis, R_{LEH} is the original LEH diameter, and σ is the Stefan-Boltzmann constant. However, not all the measured x-radiation comes from inside the hohlraum.³ The radiation temperature inside the hohlraum, T_{HOHL} is measured by flux that comes from inside the Clear Aperture, $f * F_{\text{DANTE}}$. That is,

$$f * F_{\text{DANTE}} = \sigma T_{\text{HOHL}}^4 \pi R_{\text{CL_AP}}^2 \cos \theta \quad (2)$$

Define the DANTE correction to the radiation temperature as

$$\text{DANTE_CORR} = f * (R_{\text{LEH}} / R_{\text{CL_AP}}) \quad (3)$$

Then

$$T_{\text{HOHL}} = (\text{DANTE_CORR})^{0.25} T_{\text{DANTE}} \quad (4)$$

The red symbols in Figure 6 are the DANTE_CORR for a series of NIF target shots. Although the Clear Aperture is a function of the original LEH diameter, the DANTE_CORR is not. It hovers around a value of 1.15, so the correction to the radiation temperature is about 1.04, or 10 eV for a 300 eV hohlraum.

The 870 eV image is a mapping of the time-averaged radiation flux inside the hohlraum. Notice in Figure 4b that the center of 870 eV image is brighter than the average, indicating a hotter region. This is the region of the Inner Beams (Figure 1).

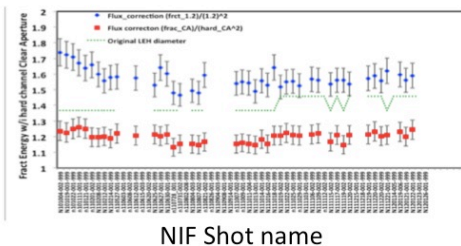


Figure 6: RED: DANTE Correction (Eq 3) using the Clear Aperture and f , fraction of flux inside the Clear Aperture. BLUE: DANTE Correction using fraction of flux inside 1.2 mm diameter circle.

The blue points in Figure 6 plot the Dante Correction for the central region, a spot 1.2 mm in diameter. These points hover around a value of 1.55, so the correction to the radiation temperature is about 1.12, or 35 eV for a 300 eV hohlraum.

Figure 7 plots the brightness (average counts/pixel) of the 870 eV image vs absorbed laser energy for two series of shots: one with 3.1 mm diameter LEHs (RED) and one with 3.37 mm diameter LEHs (BLUE). The rectangles are for a region 1.2 mm in diameter, and the Xs are within the Clear Aperture. The brightness roughly scale with laser energy. The smaller LEH hohlraums are hotter, and the central region is hotter than the average.

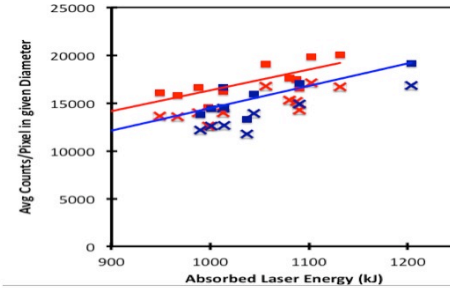


Figure 7: Plot of intensity (average counts/pixel) in 870 eV image vs absorbed laser energy for targets with (RED) 3.1 mm diameter LEHs and (BLUE) 3.37 mm LEHs. X: Average counts in Clear Aperture; (Rectangle): Average counts in 1.2 mm diameter. Lines are fits to 1.2 mm diameter data, showing the interior of the smaller LEH targets are hotter.

V. Summary

The soft x-ray channel produces a time integrated x-ray image at 870 eV, near the peak of the x-ray thermal drive. It is used to correct the measured x-radiation drive by determining the fraction of x-ray flux inside a given diameter (the “Clear Aperture” determined in the hard x-ray channel). The correction to the radiation temperature is about 10 eV, or 15% in x-ray flux. The soft image also gives a time-integrated mapping of the x-ray flux inside the hohlraum.

VI. Acknowledgements

We thank the NIF operations, laser performance, target diagnostics, data analysis, data visualization, and target fabrication teams. This work was performed under the auspices of the U.S. Department of Energy by Lawrence Livermore National Laboratory under Contract No. DE-AC52-07NA27344 and by Los Alamos National Laboratory under Contract No. DE-AC52-06NA25396.

¹E. Moses, et al., Phys.Plasmas **16**, 041006 (2009).

²J. Lindl, et al., Phys.Plasmas **11**, 339 (2004).

³N. B. Meezan, et al., IFSA paper

⁴S.H. Glenzer, et al., Science **327**, 1228 (2010). CHANGE TO MODER

⁵J. Kline, K. Widmann, A. Warrick, Rev. Sci. Instrum. **81**, 10E321 (2010)

⁶M.B. Schneider, et al., Rev. Sci. Instru. **81**, 10E538 (2010)

⁷M.D. Landon, et al., Rev. Sci. Instru. **72**, 698 (2001).

⁸M. J. Haugh and M B. Schneider., Rev. Sci. Instru **79** 10E925 (2008).

⁹REFERENCE to ALS CALIBRATION